0273-2289/98/73-2/3—0024$14.00

Analyte–Receptor Binding Kinetics for Biosensor Applications

An Analysis of the Influence of the Fractal Dimension on the Binding Rate Coefficient

AJIT SADANA

Chemical Engineering Department, University of Mississippi, University, MS 38677-9740

Received September 3, 1997; Accepted March 26, 1998

ABSTRACT

The diffusion-limited binding kinetics of antigen (analyte), in solution with antibody (receptor) immobilized on a biosensor surface, is analyzed within a fractal framework. Most of the data presented is adequately described by a single-fractal analysis. This was indicated by the regression analysis provided by Sigmaplot. A single example of a dual-fractal analysis is also presented. It is of interest to note that the binding-rate coefficient (k) and the fractal dimension (D_f) both exhibit changes in the same and in the reverse direction for the antigen–antibody systems analyzed. Binding-rate coefficient expressions, as a function of the D_f developed for the antigen–antibody binding systems, indicate the high sensitivity of the k on the D_f when both a single- and a dual-fractal analysis are used. For example, for a single-fractal analysis, and for the binding of antibody Mab 0.5β in solution to gp120 peptide immobilized on a BIAcore biosensor, the order of dependence on the D_f was 4.0926. For a dual-fractal analysis, and for the binding of 25–100 ng/mL TRITC-LPS (lipopolysaccharide) in solution with polymyxin B immobilized on a fiberoptic biosensor, the order of dependence of the binding-rate coefficients, k_1 and k_2, on the fractal dimensions, D_{f1} and D_{f2}, were 7.6335 and −11.55, respectively. The fractional order of dependence of the k(s) on the

D_f(s) further reinforces the fractal nature of the system. The k(s) expressions developed as a function of the D_f(s) are of particular value, since they provide a means to better control biosensor performance, by linking it to the heterogeneity on the surface, and further emphasize, in a quantitative sense, the importance of the nature of the surface in biosensor performance.

Index Entries: Analyte-receptor; binding coefficient; fractals; kinetics; biosensors.

INTRODUCTION

Sensitive detection systems (or sensors) are required to distinguish a wide range of substances. Sensors find application in the areas of biotechnology, physics, chemistry, medicine, aviation, oceanography, the food industry, detection of explosives (for example, buried land mines, and in aircraft luggage), and environmental control. The importance of providing a better understanding of the mode of operation of biosensors to improve their sensitivity, stability, and specificity has been emphasized *(1)*. Whetton *(2)* refers to biosensors as electronic noses, and emphasizes the reduction in time required in the detection process. For example, the Robinson test requires 48 h to determine if chocolate has absorbed any flavor from its packaging. A prototype biosensor takes 5 min for this test. The solid-phase immunoassay technique represents a convenient method for the separation and/or detection of reactants (for example, antigen) in a solution. The binding of antigen to an antibody-coated surface (or vice versa) is sensed directly and rapidly. There is a need to characterize the reactions occurring at the biosensor surface.

The details of the association of antibodies (or antigens) with antigen-coated (or antibody-coated) surface is of tremendous significance for the development and characterization of immunodiagnostic devices, as well as for biosensors *(3)*. Furthermore, external diffusional limitations play a role in the analysis of such assays *(4–6)*. The influence of diffusion in such systems has been analyzed to some extent *(5,7–13)*. The particle-enhanced sensitivity of the surface-plasmon-resonance biosensor has been analyzed *(14)*. These authors indicate that the fractal dimension (D_f) is a measure of the clustering of particles. For example, for colloidal gold, there is clustering of particles that leads to significant signal enhancement.

Kopelman *(15)* indicates that surface diffusion-controlled reactions, which occur on clusters or islands, are expected to exhibit anomalous and fractal-like kinetics. These fractal kinetics exhibit anomalous reaction orders and time-dependent rate (for example, binding) coefficients. Fractals are disordered systems, and the disorder is described by noninte-

gral dimensions *(16)*. These authors further indicate that, as long as surface irregularities show scale invariance that is dilatational symmetry, they can be characterized by a single number: D_f. The D_f is a global property, and is insensitive to structural or morphological details *(17)*.

Lee and Lee *(18)* indicate that the fractal approach has been applied to surface science, for example, adsorption and reaction processes. These authors emphasize that the fractal approach provides a convenient means to quantitatively represent the different structures and morphologies at the reaction interface. These authors analyzed simulations of Eley-Rideal diffusion-limited reactions on different fractal objects. They indicate that the primary advantage is that it permits the development of a predictive approach in the field of catalysis. They emphasize using the fractal approach to develop optimal catalyst structures. Furthermore, Markel et al. *(19)* indicate the widespread nature of fractals in nature. Fractals are present in sols and gels, soot and smoke, on rough surfaces, disordered layers on surfaces, and in porous objects.

Antibodies are heterogeneous, and their immobilization on a fiberoptic surface, for example, would exhibit some degree of heterogeneity. This is a good example of a disordered system, and a fractal analysis is appropriate for such systems. Besides, the antibody–antigen reaction on the surface is a good example of a low-dimension reaction system in which the distribution tends to be less random *(15)*. A fractal analysis would provide novel physical insights into the diffusion-controlled reactions occurring at the surface. Fractal kinetics have been reported in other biochemical reactions, such as the gating of ion channels *(20,21)*, enzyme reactions *(22)*, and protein dynamics *(23)*. It has been emphasized that the nonintegral dimensions of the Hill coefficient, used to describe the allosteric effects of proteins and enzymes, is a direct consequence of the fractal property of proteins *(22)*. Goetze and Brinkmann *(24)* have analyzed the scaling properties of 53 protein surfaces. They emphasize that these surfaces show self-similarities. Self-similarity is measured by the D_f of the surface.

Allometric scaling laws, including the metabolic reactions, have been analyzed *(25)*. These authors indicate that these laws are characteristic of all organisms. For example, they were able to describe the three-fourths power law for metabolic reactions using a model of transport of essential materials through space-filling fractal networks of branching tubes. A characteristic feature of fractals is the self-similarity at different levels of scale. When the heart rate (beats per min) of a healthy individual is recorded for 3, 30, and 300 min, the quick, erratic fluctuations seem to vary in a manner similar to the slower fluctuations *(26)*. This indicates self-similarity, which does not imply identity, but does imply that the features of a structure or process look alike at different scales of length or time.

Fractal aggregate scaling relationships have been determined for both diffusion-limited and diffusion-limited cluster aggregation (DLCA) processes in spatial dimensions, 2, 3, 4, and 5 *(27)*. These authors noted that the prefactor displays uniform trends with the D_f. Fractal dimension values for the kinetics of antigen–antibody binding *(28,29)*, and for analyte–receptor *(30)* binding for fiberoptic biosensor systems, are available. In these studies, the influence of the experimental parameters, such as analyte concentration on the D_f and on the binding-rate coefficient (k; the prefactor, in this case), were analyzed. No quantitative or direct attempt was made to relate the influence of the degree of surface roughness, such as the D_f on k. One would like to delineate the role of surface roughness on the speed of response, specificity, stability, and sensitivity of fiberoptic and other biosensors. The authors now extend these prefactor studies *(27)* to biosensor applications, wherein the D_f is initially determined and k (prefactor) for different antigen–antibody, and, in general, analyte–receptor reactions for different biosensor applications. Thereafter, quantitative relationships are presented for the k as a function of the D_f obtained for different biosensor applications. The noninteger orders of dependence obtained for the k on the D_f further reinforces the fractal nature of these analyte–receptor binding systems.

THEORY

An analysis of the binding kinetics of antigen in solution with antibody immobilized on the biosensor surface is available *(28)*. The influence of lateral interactions on the surface and variable-rate coefficients is also available *(31)*. Here the authors initially present a method of estimating actual D_f values for analyte–receptor binding systems utilized in fiberoptic biosensors.

Variable Binding-Rate Coefficient

Kopelman *(15)* has recently indicated that classical reaction kinetics is sometimes unsatisfactory, when the reactants are spatially constrained on the microscopic level by walls, phase boundaries, or force fields. Such heterogeneous reactions as, for example, bioenzymatic reactions, which occur at interfaces of different phases, exhibit fractal orders for elementary reactions and rate coefficients with temporal memories. In such reactions, the rate coefficient exhibits a form given by:

$$k_1 = k' t^{-b} \tag{1}$$

In general, k_1 depends on time, whereas, $k' = k_1 (t = 1)$ does not. Kopelman *(15)* indicates that, in three dimensions (homogeneous space), b equals zero. This is in agreement with the results obtained in classical kinetics. Also, with vigorous stirring, the system is made homogeneous and b again equals zero. However, for diffusion-limited reactions occurring in fractal spaces, $b > 0$; this yields a time-dependent rate coefficient.

The random fluctuations in a two-state process in ligand-binding kinetics has been analyzed *(32)*. The stochastic approach can be used as a means to explain the variable k. The simplest way to model these fluctuations is to assume that the $k_1(t)$ is the sum of its deterministic value (invariant) and the fluctuation ($z[t]$) *(29)*. This $z(t)$ is a random function with a zero mean. The decreasing and increasing binding rate coefficients can be assumed to exhibit an exponential form *(31,33)*:

$$k_1 = k_{1,0} exp\ (-\beta t)$$

$$k_1 = k_{1,0} exp\ (\beta t) \qquad (2)$$

Here, β and $k_{1,0}$ are constants.

The influence of a decreasing and an increasing k on the antigen concentration near the surface has been analyzed when the antibody is immobilized on the surface *(31)*. These authors noted that, for an increasing k, after a brief time interval, as time increases, the concentration of the antigen near the surface decreases, as expected for the cases when lateral interactions are present or absent. The diffusion-limited binding kinetics of antigen (or antibody or substrate), in solution with antibody (or antigen or enzyme) immobilized on a biosensor surface, has been analyzed within a fractal framework *(28,29)*. Furthermore, experimental data presented for the binding of HIV virus (antigen) to the antibody anti-HIV, immobilized on a surface, displays a characteristic ordered disorder *(34)*. This indicates the possibility of a fractal-like surface. It is obvious that the above biosensor system (wherein either the antigen or the antibody is attached to the surface), along with its different complexities, which include heterogeneities on the surface and in solution, diffusion-coupled reaction, time-varying adsorption or k, and so on, can be characterized as a fractal system. The diffusion of reactants toward fractal surfaces has been analyzed *(35–38)*. Havlin *(39)* has briefly reviewed and discussed these results.

Single-Fractal Analysis

Havlin *(39)* indicates that the diffusion of a particle (antibody [Ab]) from a homogeneous solution to a solid surface (antigen [Ag]-coated sur-

face), where it reacts to form a product (antibody–antigen complex [Ab·Ag]) is given by:

$$(Ab \cdot Ag) \sim \begin{cases} t^{(3-D_f)/2} = t^p & t < t_c \\ t^{1/2} & t > t_c \end{cases} \quad (3)$$

Here D_f is the fractal dimension of the surface. Equation 3 indicates that the concentration of the product Ab·Ag (t), in a reaction Ab + Ag → Ab·Ag on a solid fractal surface, scales at short and intermediate scales as Ab·Ag ~ t^p with the coefficient $p = (3 - D_f)/2$ at short time-scales, and $p = 1/2$ at intermediate time-scales. This equation is associated to the short-term diffusional properties of a random walk on a fractal surface. Note that, in a perfectly stirred kinetics on a regular (nonfractal) structure (or surface), k_1 is a constant, that is, it is independent of time. In other words, the limit of regular structures (or surfaces), and the absence of diffusion-limited kinetics, leads to k_1 being independent of time. In all other situations, one would expect a scaling behavior given by $k_1 \sim k' t^{-b}$ with $-b = p < 0$. Also, the appearance of the coefficient, p, different from $p = 0$, is the consequence of two different phenomena, that is, the heterogeneity (fractality) of the surface and the imperfect mixing (diffusion-limited) condition.

Havlin *(39)* indicates that the crossover value may be determined by $r_c^2 \sim t_c$. Above the characteristic length, r_c, the self-similarity is lost. Above t_c, the surface may be considered homogeneous, since the self-similarity property disappears, and regular diffusion is now present. For the present analysis, t_c is arbitrarily chosen. One may consider the analysis to be presented as an intermediate heuristic approach, in that, in the future one may also be able to develop an autonomous (and not time-dependent) model of diffusion-controlled kinetics.

Dual-Fractal Analysis

The single-fractal analysis presented above is extended to include two fractal dimensions. At present, the time ($t = t_1$) at which the first D_f changes to the second D_f is arbitrary and empirical. For the most part, it is dictated by the data analyzed and experience gained by handling a single-fractal analysis. A smoother curve is obtained in the transition region, if care is taken to select the correct number of points for the two regions. In this case, the product (antibody–antigen complex, Ab·Ag) concentration on the biosensor surface is given by:

$$(Ab \cdot Ag) \sim \begin{cases} t^{(3-D_{f1})/2} = t^{p_1} & t < t_1 \\ t^{(3-D_{f2})/2} = t^{p_2} & t_1 < t < t_2 = t_c \\ t^{1/2(3-D_{f2})/2} & t > t_c \end{cases} \quad (4)$$

RESULTS

Rogers et al. *(40)* have analyzed the pharmacological activity of a nicotinic acetylcholine receptor (nAChR) optical biosensor. They utilized three fluorescein isothiocyanate (FITC)-labeled neurotoxic peptides: α-bungarotoxin (α-BGT), α-Naja toxin (α-NT), and α-conotoxin (GI, α-CNTX). These peptides vary in their reversibility of their receptor inhibition. Nonspecific binding is a problem. Thus, these authors measured by evanescent fluorescence the nonspecific binding of α-BGT, α-NT, and α-CNTX on two sets of quartz fibers. Figure 1 shows the curves obtained using Eq. 3 for the binding of the above neurotoxic peptides. In each of these cases, a single-fractal analysis is adequate to describe the binding kinetics. Table 1A shows the values of the k and the D_f obtained. The k presented in Table 1 was obtained from a regression analysis using Sigmaplot *(41)* to model the experimental data using Eq. 3, wherein $(Ab{\cdot}Ag) = kt^p$. The k and D_f values, presented in Table 1, are within 95% confidence limits. For example, the value of k reported for the binding of FITC-α-BGT to the quartz fiber is 45.025 ± 2.389. The 95% confidence limit indicates that 95% of the k values will fall between 45.025 and 47.414. This indicates that the values are precise and significant. The curves presented in the figures are theoretical curves.

Note that, as one goes from α-BGT to α-NT, and to α-CNTX, the k increases from 45.025 to 85.649 to 1454.7, respectively. Also, the D_f values obtained exhibit an increase from 1.2336 to 1.7432 to 2.4938, respectively (in this same sequence), as one goes from α-BGT to α-NT to α-CNTX. It is of interest to note that an increase in the D_f leads to an increase in the k, even though different neurotoxic peptides are utilized. The nonspecific binding kinetics of 5 and 10 nM FITC-α-NT to another set of quartz fibers is available *(29)*. Thus, this data analysis is not repeated here. However, the k and D_f values are presented in Table 1A.

Figure 2 shows that the k increases as the D_f increases for the nonspecific binding of these neurotoxic peptides to quartz fibers. This is in accord with the prefactor analysis of fractal aggregates *(27)*. Note that the D_f is not an actual experimental variable, such as temperature or concentration, which may be directly controlled. It is evaluated and estimated from Eqs. 3 and 4. One may consider it as a derived variable. In any case, it provides

Table 1
Influence of Different Parameters on D_fs and ks for Different Antibody–Antigen and Analyte–Receptor Reaction Kinetics

Analyte concentration in solution/receptor on surface	k	D_f	k_1	k_2	D_{f1}	D_{f2}	Ref.
(a) FITC-α-BGT	45.025 ± 2.389	1.2336 ± 0.0472	na	na	na	na	*40*
FITC-α-NT	85.649 ± 11.52	1.7432 ± 0.1148	na	na	na	na	*40*
FITC-α-CNTX	1454.7 ± 48.64	2.4938 ± 0.0273	na	na	na	na	*40*
5 n*M* FITC-α-BGT	150.6 ± 9.60	1.47 ± 0.074	na	na	na	na	*40*
10 n*M* FITC-α-NT	99.1 ± 2.13	1.54 ± 0.029	na	na	na	na	*40*
(b) 10 ng/mL LPS/ polymyxin B	10.451 ± 1.836	2.7190 ± 0.1064	13.731 ± 4.612	12.094 ± 0.469	2.0236 ± 0.5908	3.00 − 0.050	*42*
25 ng/mL LPS/ polymyxin B	13.900 ± 2.207	2.6218 ± 0.0968	17.019 ± 6.169	15.384 ± 0.700	2.0932 ± 0.6310	2.6218 ± 0.0968	*42*
50 ng/mL LPS/ polymyxin B	18.433 ± 3.148	2.6528 ± 0.1036	23.571 ± 7.710	21.519 ± 0.604	2.000 ± 05772	2.9508 ± 0.0364	*42*
100 ng/mL LPS/ polymyxin B	28.34 ± 3.443	2.6792 ± 0.0754	33.939 ± 9.434	31.136 ± 0.825	2.2158 ± 0.4528	2.8633 ± 0.0344	*42*
200 ng/mL LPS/ polymyxin B	47.289 ± 3.665	2.7102 ± 0.0484	56.082 ± 5.447	51.391 ± 1.711	2.3326 ± 0.1890	2.7102 ± 0.0484	*42*
(c) Mab 0.5β diluted 1/20,000; flow rate 2 μL/min/582 RU biotinylated gp120 peptide	5.7255 ± 0.110	1.0962 ± 0.0142	na	na	na	na	*43*

Mab 0.5β; 5 μL/min/ 582 RU gp120 peptide	5.9264 ± 0.197	1.0322 ± 0.0340	na	na	na	na	*43*
Mab 0.5β; 10 μL/min/ 582 RU gp120 peptide	8.0141 ± 0.161	1.1232 ± 0.0206	na	na	na	na	*43*
Mab 0.5β; 25 μL/min/ 582 RU gp120 peptide	9.3402 ± 0.074	1.1572 ± 0.0170	na	na	na	na	*43*
Mab 0.5 β; 50 μL/min/ 582 RU gp120 peptide	10.606 ± 0.227	1.1884 ± 0.0218	na	na	na	na	*43*
Mab 0.5β; 100 μL/min/ 582 RU gp120 peptide	12.625 ± 0.141	1.2454 ± 0.0114	na	na	na	na	*43*
(d) mFab 20.5.3 diluted 1/4000; flow rate 2 μL/ min/598 RU biotinylated gp32 peptide	1.7941 ± 0.038	1.3584 ± 0.019	na	na	na	na	*43*
mFab 20.5.3; 5 μL/min/ 598 RU gp32 peptide	2.7268 ± 0.153	1.4536 ± 0.0589	na	na	na	na	*43*
mFab 20.5.3; 10 μL/min/ 598 RU gp32 peptide	1.3728 ± 0.028	1.6272 ± 0.0286	na	na	na	na	*43*
mFab 20.5.3; 25 μL/min/ 598 RU gp32 peptide	2.1789 ± 0.071	1.1746 ± 0.0345	na	na	na	na	*43*
mFab 20.5.3; 50 μL/min/ 598 RU gp32 peptide	2.9564 ± 0.196	1.2914 ± 0.0690	na	na	na	na	*43*
mFab 20.5.3; 100 μL/min/ 598 RU gp32 peptide	2.7408 ± 0.138	1.2260 ± 0.0666	na	na	na	na	*43*

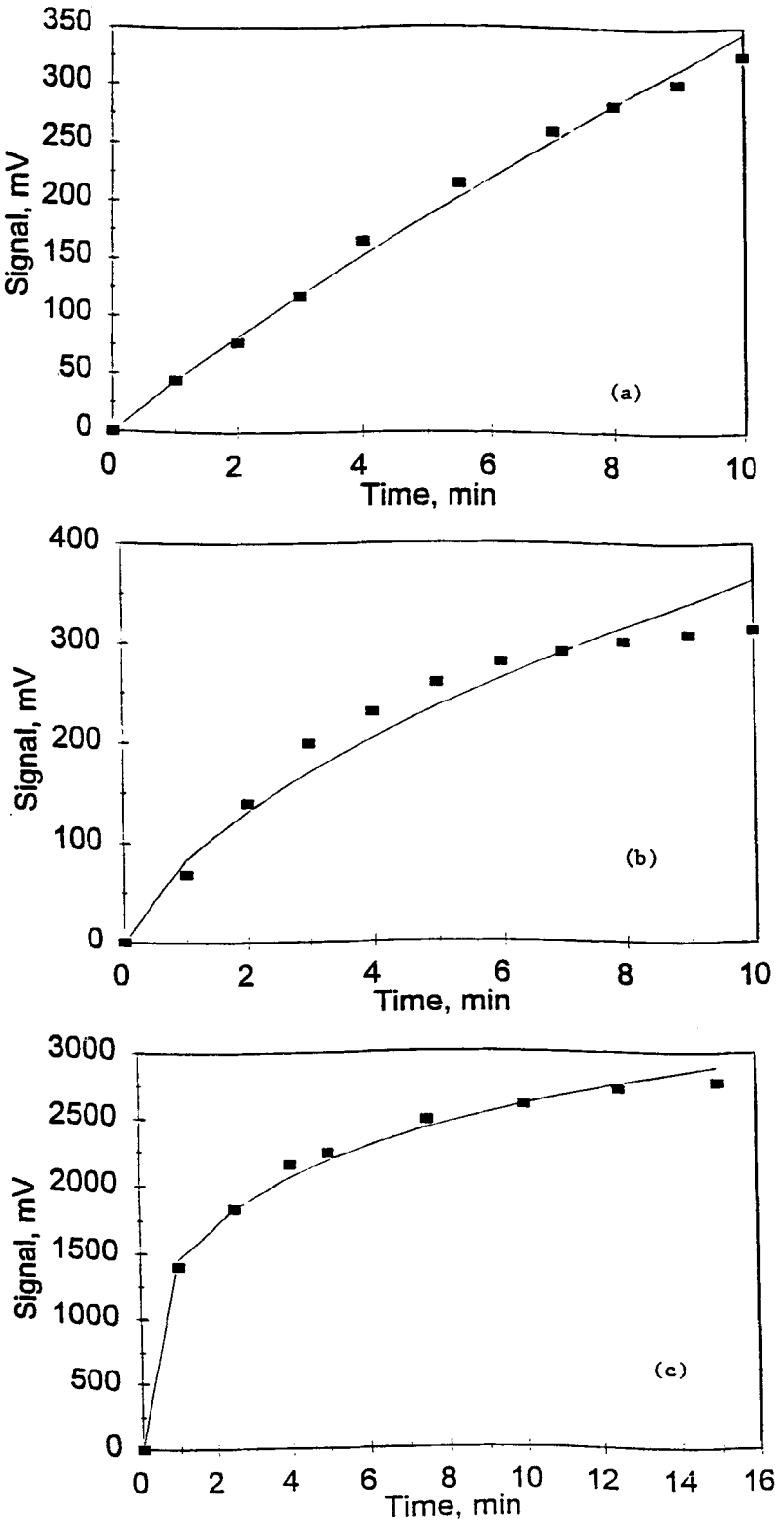

Fig. 1. Nonspecific binding of (FITC)-labeled neurotoxic peptides to quartz fibers. Adapted with permission from ref. *(40)*. **(A)** α-bungarotoxin (α-BGT), **(B)** α-*Naja* toxin (α-NT), **(C)** α-conotoxin (α-CNTX) (single-fractal analysis).

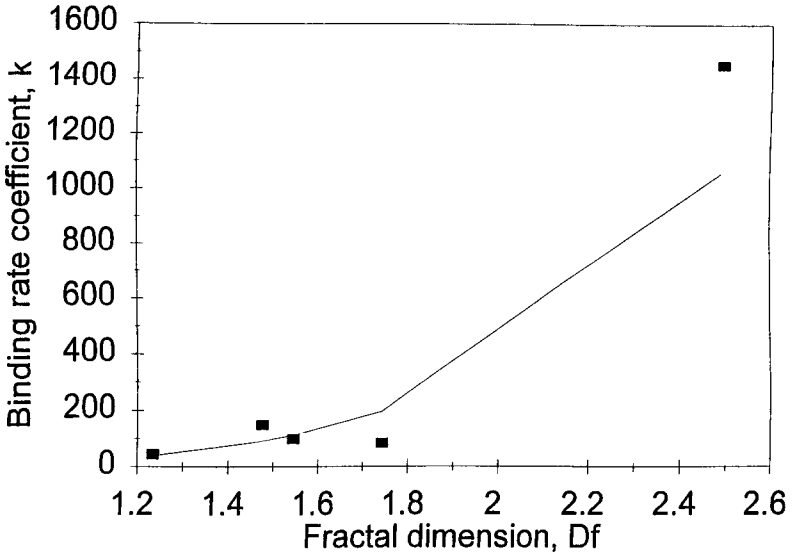

Fig. 2. Influence of the D_f on the k for the nonspecific binding of neurotoxic peptides (α-BGT, α-NT, α-CNTX) to quartz fibers *(40)*.

a quantitative estimate of the degree of heterogeneity or surface roughness. For the data presented in Table 1A, the k is given by:

$$k = (14.743 \pm 12.220)\, D_f^{4.6716 \pm 1.1513} \tag{5}$$

This predictive equation fits the values of the k presented in Table 1A, reasonably well. There is some deviation at the high fractal dimension value. Considering that data is plotted from two different sets of experiments, that is rather reasonable. Note the high exponent dependence of the k on the D_f. This underscores that the k is sensitive to the surface roughness or heterogeneity that exists on the surface. Also, the data analysis, in itself, does not provide any evidence for surface roughness or heterogeneity, and the existence of surface roughness or heterogeneity assumed may not be correct.

An evanescent fiberoptic biosensor has been developed to detect lipopolysaccharide (LPS) found in the outer cell membrane of gram-negative bacteria *(42)*. These authors analyzed the kinetics and stability of the binding of 25–200 ng/mL TRITC-LPS (also known as endotoxin) in solution with polymyxin B immobilized on the fiberoptic biosensor. Figure 3 shows the curves obtained, using Eqs. 3 and 4, for the binding of LPS in solution with the polymyxin immobilized on the biosensor. Table 1B shows the values of the binding rate coefficients obtained using a single- and a dual-fractal analysis. Figure 3 shows that, for each of the 25–200

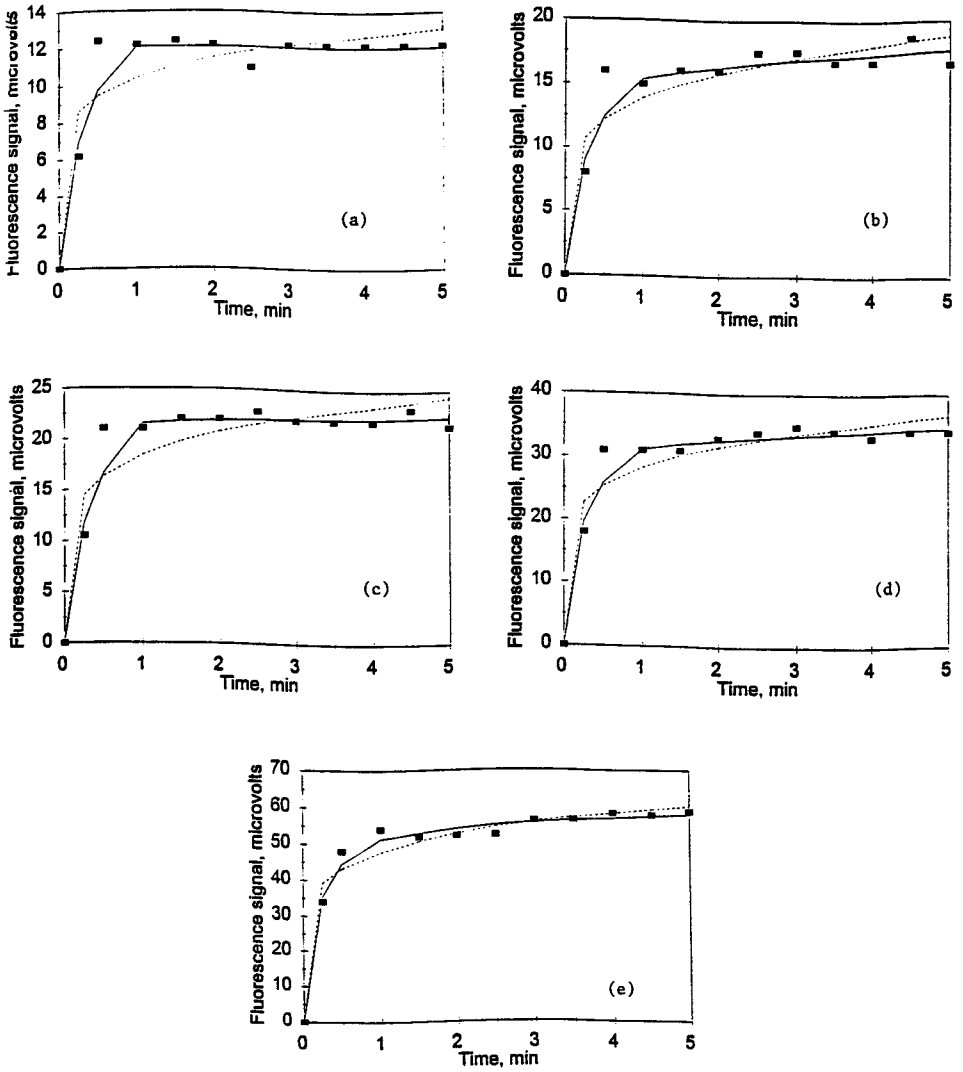

Fig. 3. Binding of different concentrations (in ng/mL) of lipopolysaccharide (TRITC-LPS) in solution to polymyxin B immobilized on a fiberoptic biosensor. Adapted with permission from ref. *(42)*. **(A)** 10; **(B)** 25; **(C)** 50; **(D)** 100; **(E)** 200. (--- single-fractal analysis; —dual-fractal analysis).

ng/mL TRITC-LPS concentrations used, a dual-fractal analysis provides a better fit than that obtained by a single-fractal analysis. Therefore, only the dual-fractal analysis is analyzed further in more detail.

Table 1B indicates that, for a dual-fractal analysis, an increase in the TRITC-LPS concentration in solution leads to an increase in the binding-rate coefficients, k_1 and k_2. Figure 4 also shows that the k_1 and k_2, increase as the TRITC-LPS concentration in solution increases. In the 25–200 ng/mL TRITC-LPS concentration utilized, the k_1 is given by:

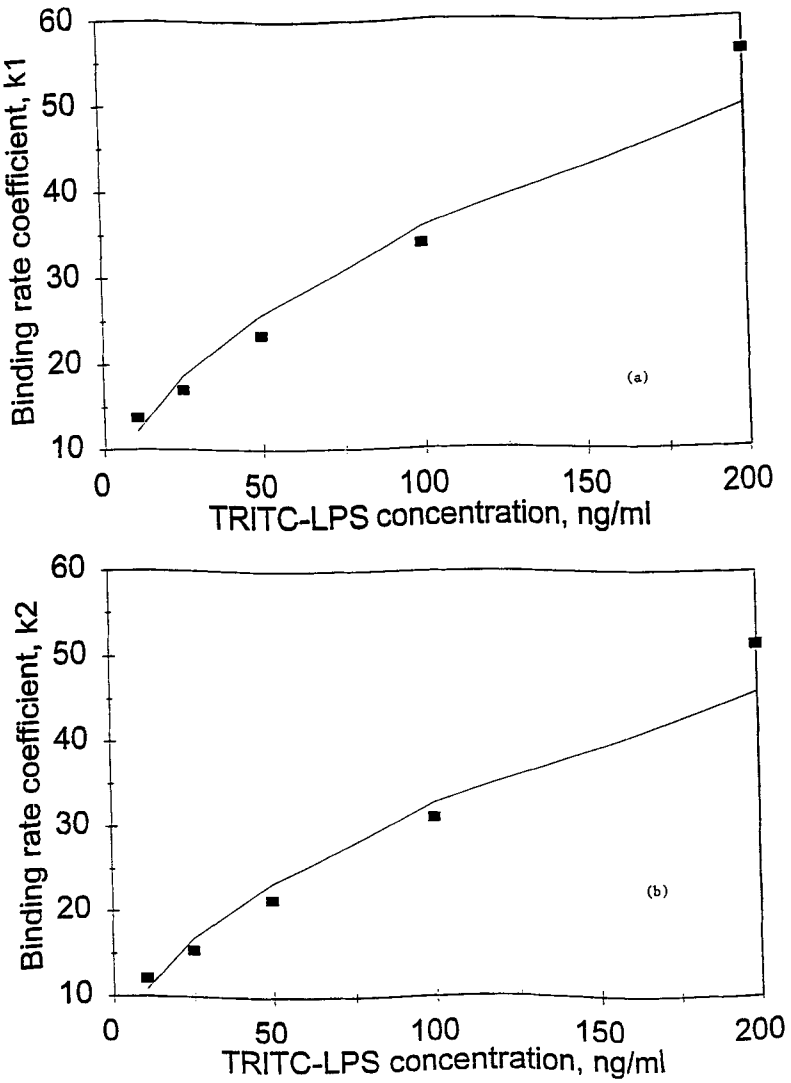

Fig. 4. Influence of the TRITC-LPS concentration in solution on the binding-rate coefficients: **(A)** k_1 and **(B)** k_2 *(42).*

$$k_1 = (4.120 \pm 0.573)\,[\text{TRITC-LPS}]^{0.4696 \pm 0.0556} \tag{6}$$

and the k_2 is given by:

$$k_2 = (3.5515 \pm 0.4574)\,[\text{TRITC-LPS}]^{0.4827 \pm 0.0518} \tag{7}$$

These predictive equations fit the value of k_1 and k_2 presented in Table 1B reasonably well. The exponent dependence of the binding-rate coefficients on the TRITC-LPS concentration in solution lends support to the fractal nature of the system.

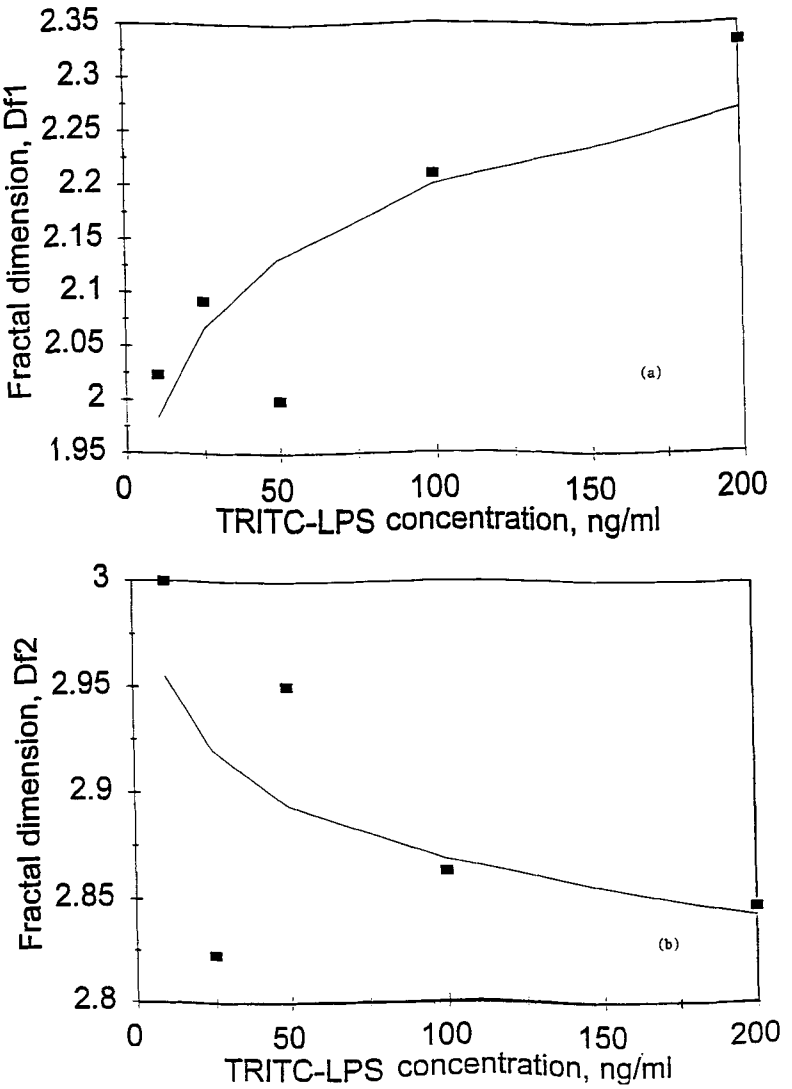

Fig. 5. Influence of the TRITC-LPS concentration in solution on the fractal dimensions: **(A)** D_{f1}; **(B)** D_{f2} *(42)*.

Figure 5A shows the influence of the TRITC-LPS concentration on the D_{f1}. An increase in the TRITC-LPS concentration in solution leads to an increase in the D_{f1}. In the 25–200 ng/mL TRITC-LPS concentration in solution utilized, the D_{f1} is given by:

$$D_{f1} = (1.7882 \pm 0.0778)\,[\text{TRITC-LPS}]^{0.04501 \pm 0.0182} \quad (8)$$

The fit of the above predictive equation is reasonable. There is some scatter in the data. More data points are required to more firmly establish the

above predictive equation. The D_{f1}, is not very sensitive to the TRITC-LPS concentration in solution, as noted by the very low exponent dependence of D_{f1} on TRITC-LPS concentration.

Figure 5B shows the influence of the TRITC-LPS concentration in solution on the D_{f2}. In the 25–200 ng/mL TRITC-LPS concentration in solution utilized, the D_{f2} is given by:

$$D_{f2} = (3.0445 \pm 0.0746)\,[\text{TRITC-LPS}]^{-0.01294 \pm 0.0103} \quad (9)$$

Note that an increase in the TRITC-LPS concentration in solution leads to a decrease in the D_{f2}. There is scatter in the data at the lower TRITC-LPS concentrations used. The scatter in the data is also indicated by the error in estimating the exponent dependence in Eq. (9). Once again, the fractal dimension, D_{f2}, is rather insensitive to the TRITC-LPS concentrations in solution, as noted by the low exponent dependence on [TRITC-LPS] in Eq. 9. More data points are required, especially at the lower TRITC-LPS concentration in solution, to more firmly establish the above predictive equation.

Figure 6A shows that the k_1, increases as the D_{f1}, increases. For the data presented in Table 1B, the k_1, is given by:

$$k_1 = (0.0793 \pm 0.0292)\, D_{f1}^{7.6335 \pm 2.4367} \quad (10)$$

The fit of the above predictive equation is reasonable. The k_1, is very sensitive to the D_{f1}, as noted by the high exponent dependence of k_1 on D_{f1}. Once again, this underscores that the k_1 is very sensitive to the surface roughness or heterogeneity that exists on the biosensor surface.

Figure 6B shows that the k_2, decreases as the D_{f2} increases. For the data presented in Table 1B, the k_2, is given by:

$$k_2 = (4.9640 \pm 3.7788)\, D_{f2}^{-11.55 \pm 10.9525} \quad (11)$$

There is scatter in the data, especially at the lower values of the D_{f2}, presented. This is reflected in both of the coefficients presented in Eq. 11. More data is required at the lower D_{f2} values, to more firmly establish the predictive equation presented above. However, the k_2, presented is still very sensitive to the D_{f2}, or to the heterogeneity that exists on the biosensor surface. Once again, the data analysis, in itself, does not provide any evidence for surface roughness or heterogeneity, and the existence of surface roughness or heterogeneity assumed may not be correct.

Richalet-Secordel et al. *(43)* have recently utilized the BIAcore biosensor to analyze the binding of ligand–analyte pairs, under conditions in which the mass transport is not totally, but only partially, rate-limiting.

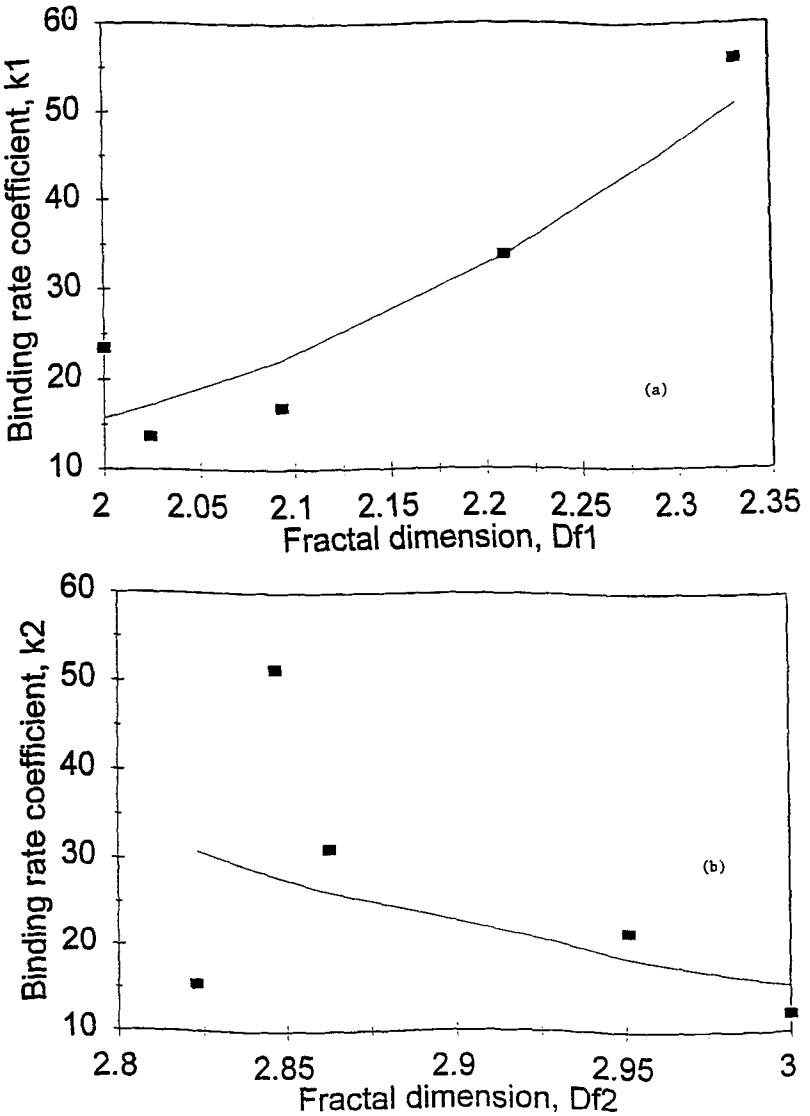

Fig. 6. Influence of **(A)** the D_{f1} on the k_1, and **(B)** the D_{f2} on the k_2 *(42)*.

They successfully used this method to measure the concentration of monoclonal antibodies and monoclonal antibody fragments (Fab). These authors utilized different flow rates of the analyte, which interacted with a ligand that is covalently linked to a dextran matrix that is bound to a biosensor surface. They indicate that the binding of the protein leads to an increase in the refractive index. This increase in the refractive index is monitored in real time by the change in the resonance angle. For these set of experiments, these authors immobilized 5860 RU of streptavidin on

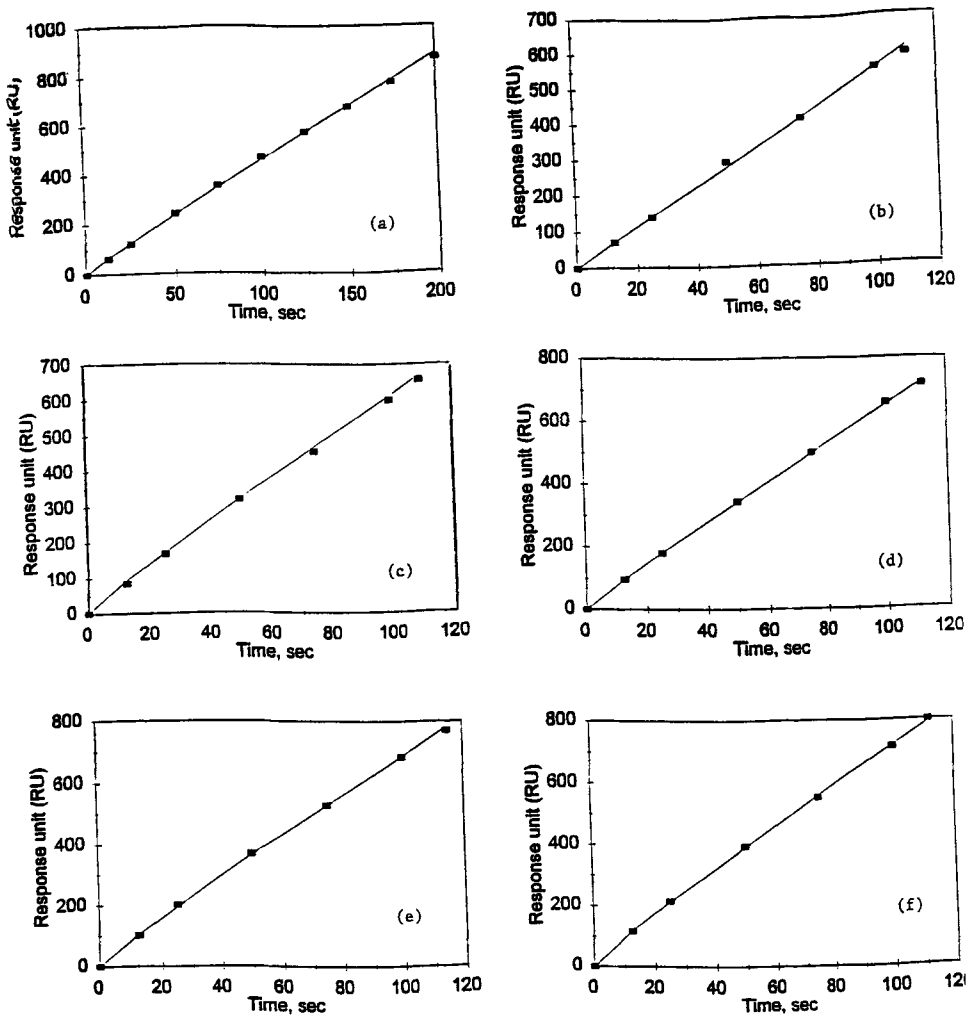

Fig. 7. Influence of different flow rates (in μL/min) on the binding of Mab 0.5β in solution to biotinylated gp120 peptide immobilized on a BIAcore biosensor: **(A)** 2; **(B)** 5; **(C)** 10; **(D)** 25; **(E)** 50; **(F)** 100. Adapted with permission from ref. *(43)*.

the dextran matrix. This was followed by 582 RU of the biotinylated gp120 peptide. Figure 7 shows the binding of Mab 0.5β in solution to the gp120 peptide. The Mab was diluted 1/20,000, and injected for 2 min at different flow rates (ranging from 2–100 μL/min) over the gp120 peptide.

Note that, in each of the cases presented in Fig. 7, a single-fractal analysis is adequate to describe the binding kinetics. Table 1C shows the values of the *k*s and the D_fs obtained for the different flow rates ranging from 2 to 100 μL/min. Table 1C indicates that an increase in the D_f leads to an increase in the *k*. This is more clearly brought out in Fig. 8, in which the

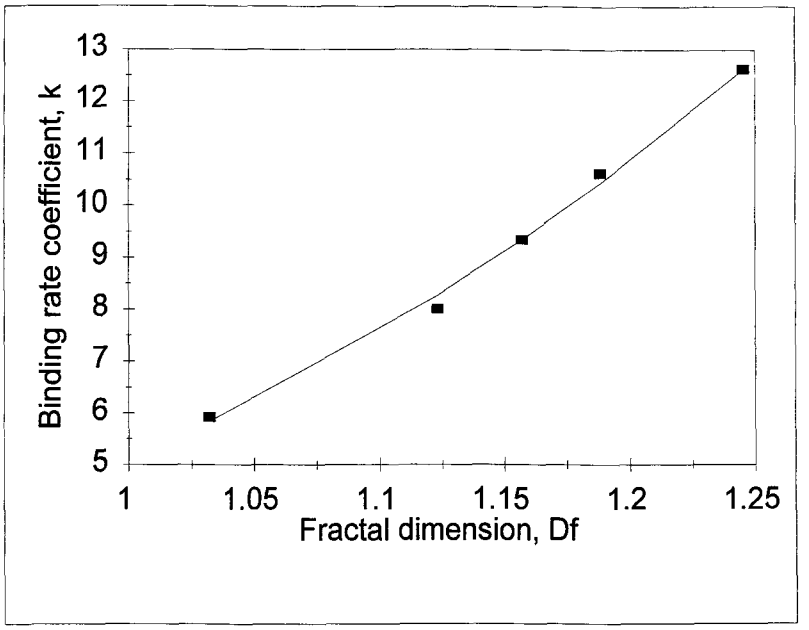

Fig. 8. Influence of the D_f, on the k *(43).*

increase in the k with an increase in the fractal dimension, D_f is more obvious. In the D_f range presented in Table 1C, the k may be represented by:

$$k = (5.1395 \pm 0.1149)\, D_f^{4.0926 \pm 0.1576} \tag{12}$$

Note that the above equation predicts the k values presented in Table 1C reasonably well. The high exponent dependence of the k on the D_f once again indicates that the k value is very sensitive to the degree of heterogeneity that exists on the BIAcore surface. The range of the D_f presented in Fig. 8 and Table 1C is rather narrow. More data points are required over a wider range of D_f values to further establish the above predictive equation (Eq. 12). As indicated earlier, the data analysis, in itself, does not provide any evidence for surface roughness or heterogeneity, and the existence of surface roughness or heterogeneity assumed may not be correct.

Richalet-Secordel et al. *(43)* also utilized the BIAcore biosensor to analyze the binding of mFab 20.5.3 in solution to biotinylated gp32 peptide (598 RU). Once again, different flow rates were used. Figure 9 shows that, for the 2–100 μL/min flow rates used, a single-fractal analysis is adequate to describe the binding kinetics. Table 1D shows the values of the k and the D_f for the different flow rates, ranging from 2–100 μL/min. For the different flow rates presented in Table 1D, the k may be represented by:

$$k = (2.331 \pm 0.541)\, D_f^{0.2110 \pm 1.1720} \tag{13}$$

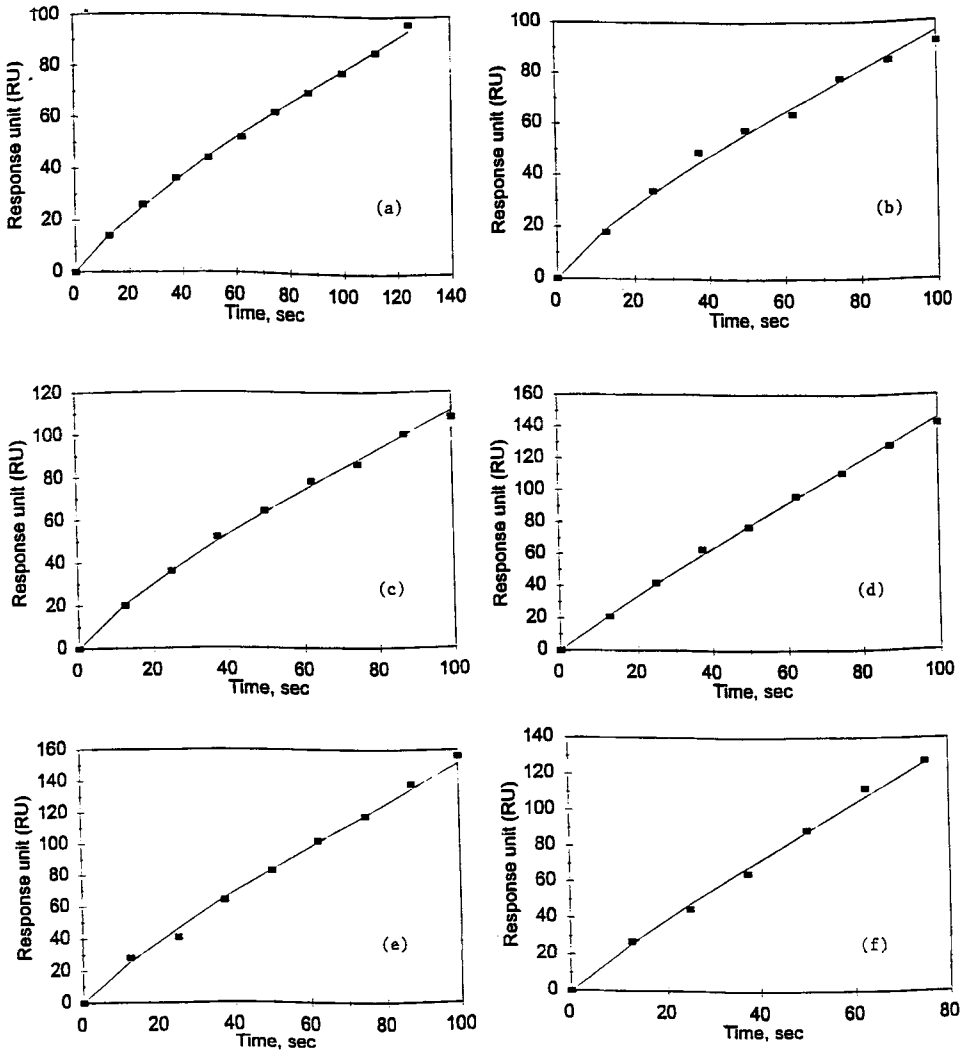

Fig. 9. Influence of different flow rates (in μL/min) on the binding of mFab 20.5.3 in solution to biotinylated gp32 peptide immobilized on a BIAcore biosensor: **(A)** 2; **(B)** 5; **(C)** 10; **(D)** 25; **(E)** 50; **(F)** 100. Adapted with permission from ref. *(43)*.

Figure 10 shows that there is considerable scatter in the data. This is clearly indicated in the error in the exponent for the D_f term in Eq. 13. More data points are required over a wider range of D_f values, to more firmly establish the above predictive equation (Eq. 13). As indicated earlier, the data analysis, in itself, does not provide any evidence for surface roughness or heterogeneity, and the existence of surface roughness or heterogeneity assumed may not be correct. However, based on the present results, and in the narrow range of D_f values analyzed, it appears that the k is only slightly sensitive to the D_f or to the degree of heterogeneity that exists on

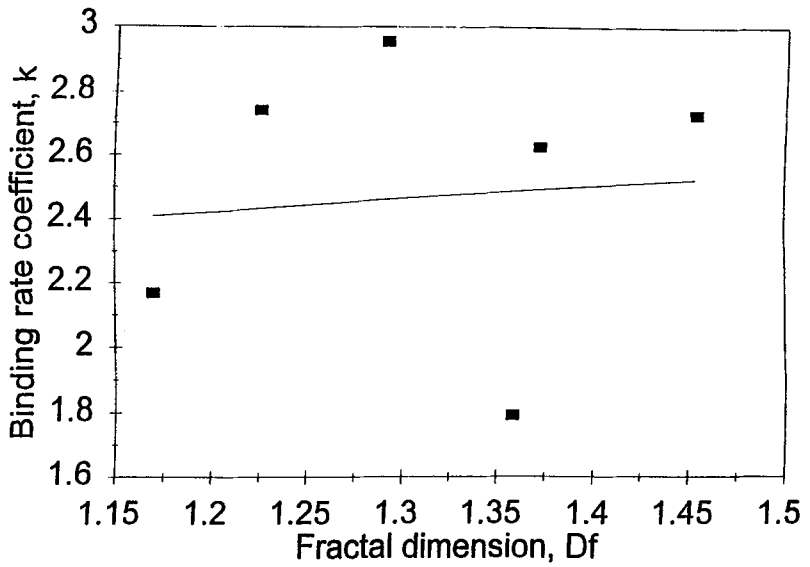

Fig. 10. Influence of the D_f on the k *(43)*.

Table 2
Binding-Rate Coefficient Expressions as a Function of the D_f and the Analyte Concentration, and D_f Expressions as a Function of the Analyte Concentration for Different Analyte–Receptor Systems

Analyte–receptor system	k or D_f expression	Ref.
(FITC)-labeled neurotoxic peptides (α-BGT, α-NT, α-CNTX)/quartz fiber 25–200 ng/mL	$k = (14.743 \pm 12.220)\ D_f^{4.6716 \pm 1.1513}$	*40*
TRITC-LPS/ polymyxin B	$k_1 = (4.120 \pm 0.573)[\text{TRITC-LPS}]^{0.4696 \pm 0.0556}$ $k_2 = (3.5515 \pm 0.4574)\ [\text{TRITC-LPS}]^{0.4827 \pm 0.0518}$ $D_{f1} = (1.7882 \pm 0.0778)\ [\text{TRITC-LPS}]^{0.04501 \pm 0.0182}$ $D_{f2} = (3.0445 \pm 0.0746)\ [\text{TRITC-LPS}]^{-0.01294 \pm 0.0103}$ $k_1 = (0.0793 \pm 0.0292)\ D_{f1}^{7.6335 \pm 2.4367}$ $k_2 = (4.9640 \pm 3.7788)\ D_{f2}^{-11.55 \pm 10.9525}$	*42*
Mab 0.5β/gp120 peptide on BIAcore biosensor (different flow rates)	$k = (5.1395 \pm 0.1149)\ D_f^{4.0926 \pm 0.1576}$	*43*
mFab 20.5.3/gp32 peptide on BIAcore biosensor (different flow rates)	$k = (2.331 \pm 0.541)\ D_f^{0.2110 \pm 1.1720}$	

the BIAcore biosensor surface. This is in contrast to the previous results presented for the binding of Mab 0.5β to the BIAcore biosensor, wherein the k is very sensitive to the heterogeneity (*see* Eq. 12) that exists on the biosensor surface. It is of interest to note that, using the same biosensor, there is so much difference in the influence of the heterogeneity on the k for two different analytes (such as Mab 0.5β and mFab 20.5.3). This indicates a considerable difference in the binding mechanism that exists on the BIAcore biosensor for these two analytes.

Table 2 summarizes the k expressions obtained as a function of the D_f for single- and dual-fractal analysis. For the single-fractal analysis binding systems presented, the order of dependence of the k on the D_f ranges from 0.2110 (mFab 20.5.3/gp32peptide system on a BIAcore biosensor) *(43)* to 4.6716 for the (FITC)-labeled neurotoxic peptides (α-BGT, α-NT, α-CNTX)/quartz fiber system *(40)*. Only a single example was presented for the dual-fractal analysis system. In this case (25 to 200 ng/mL TRITC-LPS/polymyxin B system: *(42)*, the k expressions for k_1 and k_2 as a function of the TRITC-LPS concentration in solution, were also presented. This table does provide an overall perspective on the nature of the dependence of the k(s) on the D_f(s) for different biosensor applications. More data needs to be analyzed to further delineate this dependence.

CONCLUSIONS

A fractal analysis of the binding of antigen (analyte) in solution to the antibody (receptor) immobilized on the biosensor surface provides a quantitative indication of the state of the disorder (D_f) and the k on the surface. The D_f value provides a quantitative measure of the degree of heterogeneity that exists on the surface for antibody–antigen (or, in general, analyte–receptor) systems. In three of the four examples presented, a single-fractal analysis provides an adequate fit. This was done by the regression analysis provided by Sigmaplot *(41)*. Only in a single case was a dual-fractal analysis required to provide an adequate fit. For the dual-fractal analysis, both the binding rate coefficients, k_1 and k_2, and the fractal dimensions, D_{f1} and D_{f2} are initially related to an experimental variable, for example, analyte concentration in solution. Then, in accord with the prefactor analysis for fractal aggregates *(27)*, quantitative expressions are developed for the k as a function of the fractal dimension, D_f for a single-fractal analysis, and for the k_1 and k_2 as a function of D_{f1} and D_{f2}, respectively, for a dual-fractal analysis. Perhaps it is more appropriate to develop an expression for k_1 as a function of D_{f1} only, and the expression for k_2 should include D_{f1} and D_{f2}. This is an initial study, and more data is required to further test if this is really required.

The D_f is not a classical independent variable, such as analyte concentration. Nevertheless, the expressions obtained for the k(s) for single- and dual-fractal analysis, as a function of the D_f(s), indicate the high sensitivity of the k(s) on the D_f(s). This is clearly brought out by the high order and fractional dependence of the k(s) on the D_f(s). For example, in the case of the single-fractal analysis, and for the nonspecific binding of FITC-labeled neurotoxic peptides (α-BGT, α-NT, and α-CNTX) to quartz fibers, and for the binding of Mab 0.5β to gp120 peptide immobilized on a BIAcore biosensor, the orders of dependence on D_f were 4.6716 and 4.0926, respectively. This emphasizes the importance of the extent of heterogeneity on the biosensor surface and its impact on the k. As indicated earlier, the data analysis, in itself, does not provide any evidence for surface roughness or heterogeneity, and the existence of surface roughness or heterogeneity assumed may not be correct. However, for the dual-fractal analysis example presented, and for the binding of 25–200 ng/mL TRITC-LPS to polymyxin B immobilized on a fiberoptic biosensor, the order of dependence of k_1 on D_{f1} was 7.6335, and of k_2 on D_{f2} was −11.55. Once again, these orders of dependence underscore the importance of the degree of heterogeneity on the biosensor surface, and its impact on the k. Table 2 summarizes the k expressions obtained as a function of the D_f for different systems utilized in biosensor applications.

In four of the five cases presented, the k increases as the D_f, or the degree of heterogeneity, increases on the biosensor surface. This was noted for the single- and dual-fractal analysis presented. More examples need to be analyzed to see if this is true for other systems (both antigen–antibody, and, in general, analyte–receptor) utilized in biosensor applications. For a single example, however, for the binding of 25–200 ng/mL TRITC-LPS to polymyxin B immobilized on a fiberoptic biosensor, k_2 decreases as the D_{f2} increases.

This is apparently the first study in which the k is directly related to the D_f, or to the degree of heterogeneity that exists on the biosensor surface. The analysis provides physical insights into the antigen–antibody reactions occurring on the biosensor surface. In general, the analysis is extendable to analyte–receptor reactions occurring on biosensor surfaces. The quantitative expressions developed for the different antigen–antibody systems should assist in the better control of the biosensor performance parameters, such as stability, selectivity, sensitivity, and response time. More detailed and precise studies are required to determine the influence of the degree of heterogeneity that exists on the biosensor surface on the k.

An increase in the k value should lead to enhanced sensitivity, and to a decrease in the response time of the biosensor. Both of these aspects would be beneficial in biosensor construction.

For a selective (or multiple) reaction system, if an increase in the D_f value leads to an increase in the k (of interest), then this would enhance selectivity. Stability is a more complex issue, and one might intuitively anticipate that a distribution or heterogeneity that exists on the biosensor surface would lead to a more stable sensor. Similar behavior has been observed for the deactivation of enzymes, wherein a distribution of activation energies for deactivation (compared to a single activation energy for deactivation) leads to a more stable enzyme *(44)*. Another parameter that is not considered (or rarely) in the biosensor literature, but often in control theory, is robustness *(R. Price, personal communications)*. This may be defined as insensitivity to measurement errors, as far as biosensor performance is concerned. At this point, it is difficult to see how D_f and k would affect biosensor robustness.

REFERENCES

1. Scheller, F. W., Hintsche, R., Pfeifer, D., Schubert, D., Rediel, K., and Kindevater, R., (1991). *Sensors Actuators* **4,** 197–206.
2. Whetton, C. (1977). *Instrument. Technol.*, August, 24.
3. Pisarchick, M. L., Gesty, D., and Thompson, N. L. (1992). *Biophys. J.* **63,** 215–223.
4. Bluestein, B. I., Craig, M., Slovacek, R., Stundtner, L., Uricouli, C., Walziak, I., and Luderer, A. (1991). In *Biosensors with Fiberoptics* (Wise, D., and Wingard, L. B., Jr., eds.), Humana, Clifton, NJ, pp. 181–223.
5. Eddowes, M. J. (1987/1988). *Biosensors* **3,** 1–15.
6. Place, J. F., Sutherland, R. M., Riley, A., and Mangan, C. (1991). In *Biosensors with Fiberoptics* (Wise, D., and Wingard, L. B., Jr., eds.), Humana, Clifton, NJ, pp. 253–291.
7. Stenberg, M., Stiblert, L., and Nygren, H. A. (1986). *J. Theor. Biol.* **120,** 129–142.
8. Nygren, H. A., and Stenberg, M. (1985). *J. Colloid Interface Sci.* **107,** 560–566.
9. Stenberg, M., and Nygren, H. A. (1982). *Anal. Biochem.* **127,** 183–192.
10. Sadana, A., and Sii, D. (1992). *J. Colloid Interface Sci.* **151,** 166–177.
11. Sadana, A., and Sii, D. (1992). *Biosens. Bioelectron.* **7,** 559–568.
12. Sadana, A., and Madagula, A. (1994). *Biosens. Bioelectron.* **9,** 45–55.
13. Sadana, A., and Beela Ram, A. (1995). *Biosens. Bioelectron.* **10,** 301–316.
14. Leung, P. T., Pollardknight, D., Malan, G. P., and Finlan, M. F. (1994). *Sensors Actuators B* **22,** 175–185.
15. Kopelman, R. (1988). *Science* **241,** 1620–1626.
16. Pfeifer, P., and Obert, M. (1989). In *Fractal Approach to Heterogeneous Chemistry: Surfaces, Colloids, Polymers* (Avnir, D., ed.), J. Wiley, New York, pp. 11–43.
17. Pajkossy, T., and Nyikos, L. (1989). *Electrochim. Acta* 34, 171–179.
18. Lee, C. K., and Lee, S. L. (1995). *Surface Sci.* **325,** 294–312.
19. Markel, V. A., Muratov, L. S., Stockman, M. I., and George, T. F. (1991). *Phys. Rev. B.* **43**(10), 8183–8189.
20. Liebovitch, L. S., and Sullivan, J. M. (1987). *Biophys. J.* **52,** 979–988.
21. Liebovitch, L. S., Fischbarg, J., Koniarek, J. P., Todorova, I., and Wang, M. (1987). *Math. Biosci.* **84,** 37–68.
22. Li, H., Chen, S., and Zhao, H. (1990). *Biophys. J.* **58,** 1373–1380.

23. Dewey, T. G., and Bann, J. H. (1992). *Biophys. J.* **63,** 594–598.
24. Goetze, T., and Brinkmann, J. (1992). *Biophys. J.* **61**, 109–116.
25. West, G. B., Brown, J. H., and Enquist, B. J. (1997). *Science* **276,** 122–126.
26. Goldberger, A. L., Rigney, D. R., and West, B. R. (1990). *Sci. Am.* February, 43–52.
27. Sorenson, C. M., and Roberts, G. C. (1997). *J. Colloid Interface Sci.* **186,** 447–456.
28. Milum, J., and Sadana, A. (1997). *J. Colloid Interface Sci.* **187,** 128–139.
29. Sadana, A. (1997). *J. Colloid Interface Sci.* **190,** 232–240.
30. Sadana, A., and Sutaria, M. (1997). *Biophys. Chem.* **65,** 29–42.
31. Sadana, A., and Madagula, A. (1993). *Biotechnol. Prog.* **9,** 259–266.
32. Di Cera, E. (1991). *J. Chem. Phys.* **95,** 5082–5089.
33. Cuypers, P. A., Willems, G. M., Kop, J. M., Corsel, J. W., Jansen, M. P., and Hermens, W. T. (1987) in *Proteins at Interfaces. Physicochemical and Biochemical Studies* (Brash, J. L. and Horbett, T. A., eds.), American Chemical Society, Washington, DC, pp. 208–211.
34. Anderson, J. (1993) *NIH Panel Review Meeting,* Case Western Reserve University, Cleveland, OH, July.
35. Sadana, A., and Beelaram A. (1995) *Biosens. Bioelectron.* **10,** 1567–1575.
36. Sadana, A. (1995) *Biotechnol. Progr.* **11,** 50–57.
37. Sadana, A., and Beelaram, A. (1994) *Biotechnol. Prog.* **10,** 291–298.
38. Sadana, A., and Sutaria, M. (1997) *Appl. Biochem. Biotechnol.* **62**(2–3), 275–290.
39. Havlin, S. (1989) in *Fractal Approach to Heterogeneous Chemistry: Surfaces, Colloids, Polymers* (Avnir, D., ed.), Wiley, New York, pp. 251–269.
40. Rogers, M. and Edelfrawi, M. (1991) *Biosens. Bioelectron.* 6, 46–56.
41. Jandel Scientific (1993), *Sigmaplot, Scientific Graphing Software, User's Manual,* San Rafael, CA.
42. James, E. A., Schmeltzer, K., and Ligler, F. S. (1996) *Appl. Biochem. Biotechnol.* **60,** 180–189.
43. Richalet-Secordel, P. M., Rauffer-Bruyere, N., Christensen, L. L. H., Ofenloch-Haehnle, B., Seidel, C., and Van Regenmortel, M. H. V. (1997) *Anal. Biochem.* **249,** 165–175.
44. Malhotra, A., and Sadana, A. (1987) *Biotech. Bioeng.* **30,** 717–725.